Springer

KSME

Journal of Mechanical Science and Technology 27 (7) (2013) 1957~1962
www.springerlink.com/content/1738-494x
DOI 10.1007/s12206-013-0516-x

Numerical analysis of the influence of electrode position on fluid flow in 2-D rectangular duct flow †

Suwimon Saneewong Na Ayuttaya, Chainarong Chaktranond* and Phadungsak Rattanadecho

Department of Mechanical Engineering, Faculty of Engineering, Thammasat University (Rangsit Campus), Pathumthani 12120, Thailand

(Manuscript Received July 20, 2011; Revised February 5, 2013; Accepted March 24, 2013)

Abstract

This paper numerically examines the influence of electrode arrangements and number of electrodes on fluid flow under electric field. The distance between the electrode and ground positions varies in the vertical direction (i.e., $H = -1$ cm to 1 cm) and horizontal direction (i.e., $L = 2$ cm to 8 cm). Electrical voltage and inlet velocity are employed at 20 kV and 0.5 m/s, respectively. Numerical results show that swirling flow occur at $H \neq 0$ cm and its direction depends on the location of H. When the distance L decreases, the swirling becomes smaller and the vorticity becomes stronger because of the higher and denser electric field intensity. Increasing the number of electrodes also increases the electric field, thus causing larger and more violent swirling. Comparisons of the flow visualization show that the simulation results are in good agreement with the experiment results.

Keywords: Electric field; Swirling flow; Electrode arrangement; Rectangular duct flow; Numerical analysis

1. Introduction

Conventional hot-air drying is simple and widely used in food preservation. However, this approach requires a long drying period, thus resulting in large energy consumption. Therefore, hot-air drying is combined with other external energy sources, such as microwave [1, 2], infrared [3, 4], and electric force or electrohydrodynamic (EHD) systems [5-7], which use electric force to control the hot-air flow structure and enhance the convective heat transfer on the product surface. The mechanism of the Corona wind is explained as follows. The ion generated by the corona discharge near the sharp electrode moves to the ground when the electric field is exposed to airflow. Therefore, ionized air moves from the electrode to the ground and conducts the shear flow caused by the difference in fluid velocity between the charged and uncharged airflows. Consequently, the shear flow induces a swirling flow [8].

The modification of flow patterns with EHD has been extensively studied by many researchers. Saneewong Na Ayuttaya et al. [8] numerically examine the effect of ground wire and ground plate on flow. Their results show that ground plate produces a wider swirling than ground wire. However, ground wire can cause stronger swirling in a specific location. Kasayapanand [9] studies heat transfer enhancement in a channel installed with an electrode bank. The results show that heat transfer performance depends on the electrode distance ratio, electrode number per length, and channel dimension. Chaktranond and Rattanadecho [11] investigate the enhancement of heat and mass transfer in the convective drying of a porous packed bed. Their experiments show that the convective heat transfer coefficient and drying rate are enhanced considerably by the EHD effect on the flow above the packed beds. In the current study, we investigate airflow that is subjected to EHD in a rectangular duct. The effects of electrode position and number of electrodes on fluid flow are also systematically investigated.

2. Computational model

The computational simulation domain is 0.15 m (high) × 0.64 m (long) (Fig. 1). Electrode and ground wires are assumed to be arranged in a circle with a diameter of 0.5 mm,

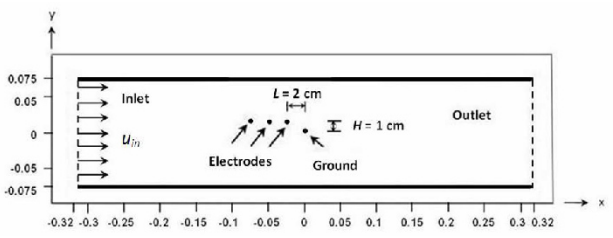

Fig. 1. Computational models: $n = 3$.

*Corresponding author. Tel.: +66 2 564 3001 ext. 3144
E-mail address: cchainar@engr.tu.ac.th
† Recommended by Associate Editor Gihun Son

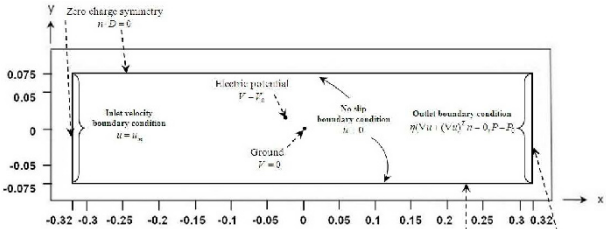

Fig. 2. Boundary conditions of the flow and electric field domains used in the analysis.

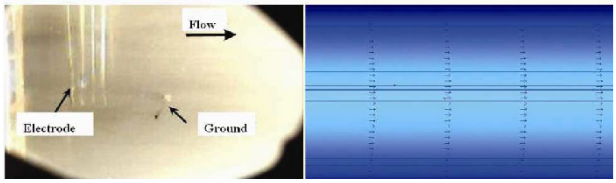

(a) (b)

Fig. 3. Comparison of the fluid motion without electric field: (a) experimental results; (b) simulated results.

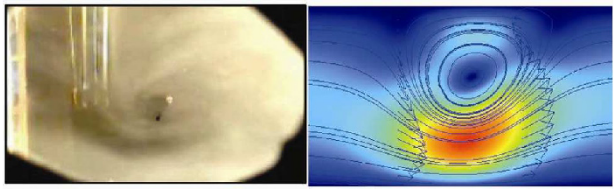

(a) (b)

Fig. 4. Comparison of fluid motion under electric field in (a) the experiments; (b) simulations.

and the ground is fixed at x = 0 m and y = 0 m. The space charge density at the tip of the electrode (q_0) is considered from David [12]. The electrode positions are based on the ground position, and the wire electrodes are varied in horizontal (L) and vertical (H) directions. Electrodes (n) are installed in the horizontal direction at the same height as the other electrodes (Fig. 2).

3. Equations

3.1 Electric field calculation

In this study, the dielectric properties are constant, and the effect of the magnetic field is negligible. The electric field distribution is computed from Maxwell's equations:

$$\nabla \cdot \varepsilon \vec{E} = q \tag{1}$$

$$\vec{E} = -\nabla V \tag{2}$$

$$\nabla \cdot J = 0 \tag{3}$$

$$J = qb\vec{E} + q\vec{u} \tag{4}$$

where ion mobility b is 1.80 × 10^{-4} m^2/V.s., and fluid permittivity (ε) is 8.85 × 10^{-12} F/m. The electric force per unit volume (F_E) on the fluid flow is computed from the electrophoretic force or Coulomb force resulting from the net uncharged force within the fluid or ions injected from the electrodes:

$$\vec{F}_E = q\vec{E}\,. \tag{5}$$

The boundary conditions for solving the electric field (Fig. 2) are considered zero-charge symmetry boundary conditions:

$$n \cdot D = 0\,. \tag{6}$$

The electric flux density is related to the electric field (E) and dielectric permittivity (ε):

$$D = \varepsilon E\,. \tag{7}$$

The electrical voltage at the electrode and ground positions are $V = V_0$ and $V = 0$, respectively.

3.2 Flow field calculation

The properties of air are assumed constant. The air is single phase and has an incompressible flow. The combination of the Navier-Stokes equations and Coulomb force equation yields the following expression:

$$\nabla \cdot \vec{u} = 0 \tag{8}$$

$$\rho(\vec{u} \cdot \nabla \vec{u}) = -\nabla \vec{P} + \mu \nabla^2 \vec{u} + \vec{F}_E \tag{9}$$

where viscosity (μ) is 1.8 × 10^{-5} kg/ms, and density (ρ) is 1.206 kg/m^3. The strength of the swirling flow subjected to the electric field is assessed through vorticity (ω):

$$\vec{\omega} = \nabla \times \vec{u}\,. \tag{10}$$

The pressure at the outlet is the atmospheric pressure (P_0), and no viscous stress is used:

$$\eta(\nabla u + (\nabla u)^T n = 0 \quad \text{and} \quad P = P_0 \tag{11}$$

where T is the transposed matrix. The upper and lower ends of the rectangular duct flow are considered the no slip boundary condition.

The computational scheme for this study requires the assembly of a finite element model by using a collocation method. The model of the Coulomb force and Navier-Stokes equation are then solved by using COMSOL. The system of governing equations is solved by using the unsymmetrical multi-frontal method. This convergence test results in a mesh with approximately 5,000 elements.

4. Results and discussion

4.1 Fluid flow under electric field

Figs. 3 and 4 show the influence of electric field on fluid

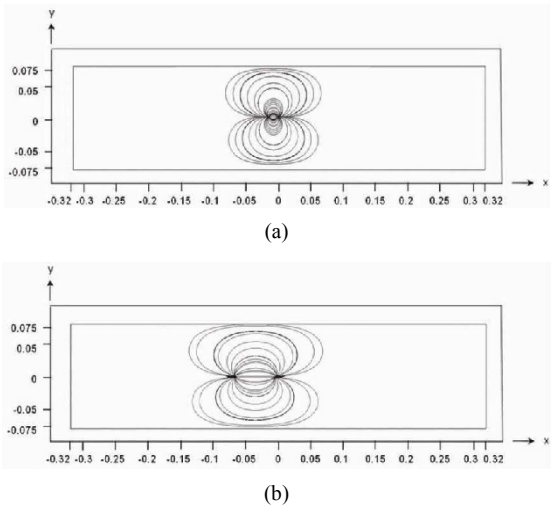

Fig. 5. Electric field in various L when H = 0 cm (V_0 = 20 kV and u_{in} = 0.5 m/s): (a) L = 2 cm; (b) L = 6 cm.

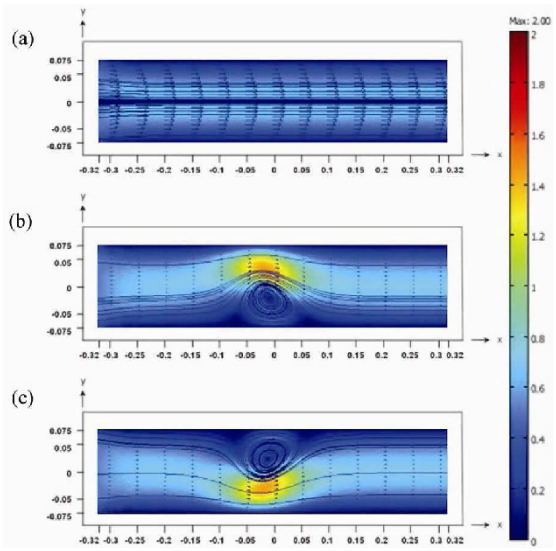

Fig. 6. Swirling flow in various H when L = 2 cm (V_0 = 20 kV and u_{in} = 0.5 m/s): (a) H = 0 cm, (b) H = −1 cm; (c) H = 1 cm.

flow from experiments conducted by Chaktranond and Rattanadecho [11] and the simulations in the current study.

The distance between the electrode and the ground in the vertical direction or elevation (H) and horizontal direction or gap (L) are fixed at 1 and 4 cm, respectively. The uniform velocity (u_{in}) of 0.1 m/s is introduced at the inlet. The swirling flow cannot be observed without electric force. When the electric field is applied at V_0 = 10 kV, swirling is clearly displayed near the electrode and the ground. This swirling also follows a counterclockwise direction. The comparison of the results shows that both techniques are in good agreement.

4.2 Effect of single electrode

Fig. 5 shows the electric field from a single electrode, where gap (L) varies. In this simulation, H = 0 cm, V_0 = 20 kV, and u_{in} = 0.5 m/s. Figs. 5(a) and 5(b) show the electric field when L = 2 and 6 cm, respectively. The electric field moves outward from the electrode to the ground and is concentrated at both the electrode and the ground, that is, $E \propto L^{-2}$.

The effect of the position of the electrode in the elevation (H) is shown in Fig. 6. When H = 0 cm, no swirling is observed (Fig. 6(a)). However, when $H \neq 0$ cm (Figs. 6(b) and 6(c)), a swirling flow occurs around the ground because of the shear flow effect resulting from the velocity difference between the fluid inertia force and electric force on uncharged airflow. However, the maximum velocity (u_{max}) in the region near the ground changes with varying elevations. For H = 0 cm and $H \neq 0$ cm (H = 1, −1 cm), u_{max} is 0.708 and 1.472 m/s. The electrode position also affects the swirling direction. Furthermore, swirling occurs in the lower wall when H = −1 cm in the clockwise direction. The swirling flow effect causes the effective area of the main flow to become smaller. At H = 1 cm, u_{max} decreases when the gap increases (Fig. 7). When L = 4, 6, and 8 cm, u_{max} is 1.225, 1.109, and 1.055 m/s, respectively. Thus, u_{max} is inversely proportional to the square

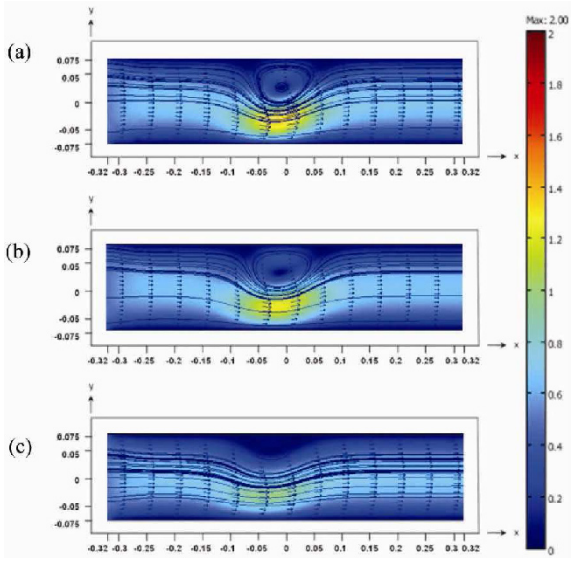

Fig. 7. Swirling flow in various gaps (V_0 = 20 kV and u_{in} = 0.5 m/s): (a) L = 4 cm; (b) L = 6 cm; (c) L = 8 cm.

of L, that is, $u_{max} \propto L^{-2}$.

Fig. 8 shows that H = 1 cm and that the gap varies from 2 cm to 8 cm. When the gap becomes smaller, vorticity occurs in the narrow zone. In each case, the maximum vorticity area occurs between the electrode and the ground zone. When the gap is reduced, the swirling flow becomes smaller but vorticity (ω) increases.

4.3 Effect of multiple electrode positions

Fig. 9 shows the effect of multiple electrodes (n) in the simulation when H = 1 cm, V_0 = 20 kV, and u_{in} = 0.5 m/s.

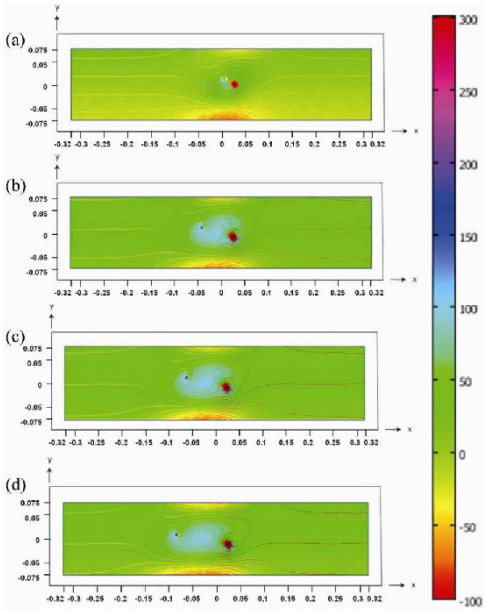

Fig. 8. Vorticity contour in various gaps when H = 1 cm: (a) L = 2 cm; (b) L = 4 cm; (c) L = 6 cm; (d) L = 8 cm.

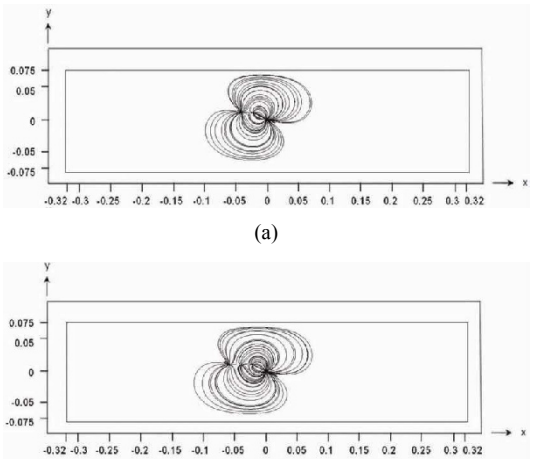

Fig. 9. Electric field when H = 1 cm (V_0 = 20 kV and u_{in} = 0.5 m/s): (a) n = 2; (b) n = 3.

When n = 3 (Fig. 9(b)), the electric field is more concentrated. Increasing the number of electrode increases the magnitude of the electric field. The maximum magnitude of the electric field occurs between the electrodes and the ground because of the high gradient of the electrical voltage.

Increasing the number of electrodes increases the swirling size (Fig. 10). In practice, a bigger swirling enhances the convective surface heat transfer area between the product and hot-air flow [11]. For n = 2 and 3, u_{max} is 1.803 and 1.951 m/s, respectively. Fig. 11 also shows that increasing the number of electrodes increases the swirling size. The maximum vorticity appears near the ground and has different locations.

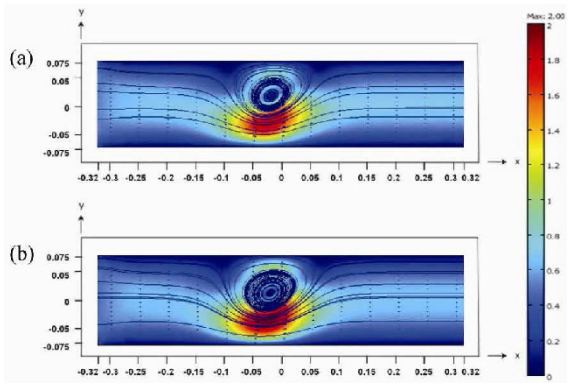

Fig. 10. Swirling flow in various electrode numbers (n) when H = 1 cm (V_0 = 20 kV and u_{in} = 0.5 m/s): (a) n = 2; (b) n = 3.

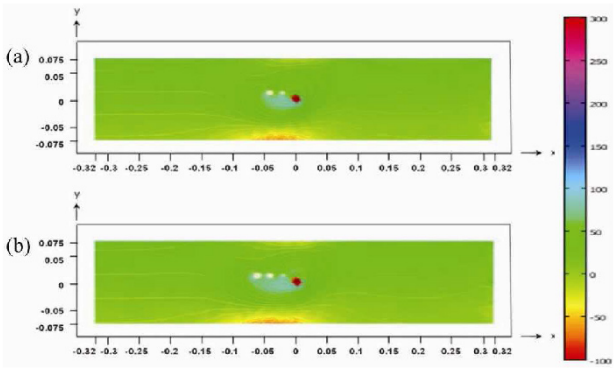

Fig. 11. Vorticity contour in various n: (a) n = 2; (b) n = 3.

4.4 Comparison of the effects of swirling flow between the simulation and experimental results

Flow visualization is based on the incense smoke technique with vector form (Figs. 12(a) and 12(e)). H = 1 cm, L = 2 cm, u_{in} = 0.5 m/s, and V_0 = 20 kV.

The results show that the swirling flow occurs above the electrode and the ground. Given that the electric force moves from multiple electrodes to the ground, the motion of swirling flow exhibits a counterclockwise direction. Furthermore, u_{max} occurs between the electrodes and the ground. Considering the limited measurements in high voltage electric field, the velocity field magnitude is assessed through the simulations (Figs. 12(f)~12(j)). When n = 1, 2, 3, 4, and 5, u_{max} is 1.472, 1.803, 2.03, 2.15, and 2.27 m/s, respectively. When multiple electrodes and a single ground are used, the space charge density from each electrode induces different shear flows. In the above data, the electric field (E) intensity depends on the distance between the electrode and the ground. The electric field weakens when the gap is larger. These results indicate that the multiple electrodes provide a larger surface for convection heat transfer.

5. Conclusions

Numerical simulation is conducted to study the influences

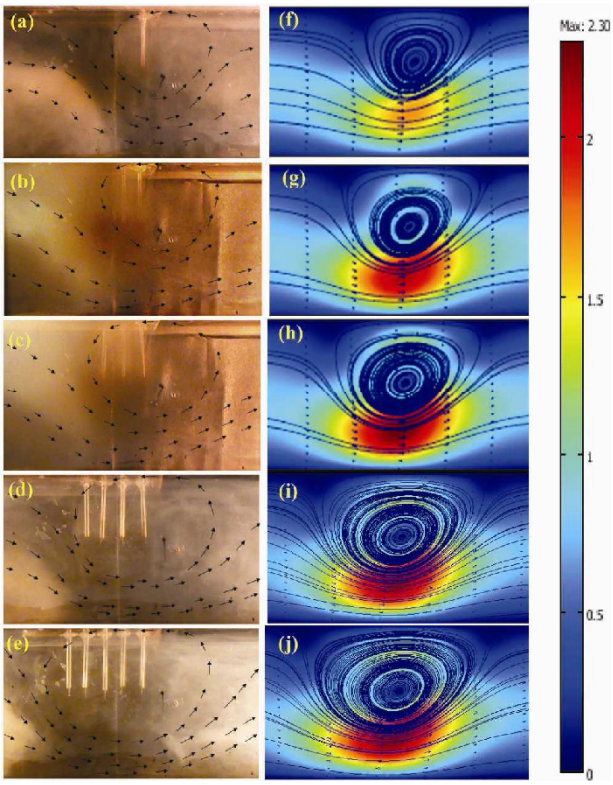

Fig. 12. Swirling flow in various n when V_0 = 20 kV, u_i = 0.5 m/s, L = 2 cm, and H = 1 cm: (a to e) incense smoke technique motion with vector form when n = 1, 2, 3, 4, and 5; (f to j) simulation results when n = 1, 2, 3, 4, and 5.

of the arrangement and the number of electrodes on the fluid flow in a rectangular duct. This electric discharge converts electrical energy into kinetic energy to reconstruct and accelerate airflow. The following conclusions are obtained from the results:

A smaller distance between the electrode and the ground causes the Coulomb force to become stronger, thus resulting in higher vorticity strength. Inversely, a larger gap widens and weakens the swirling flow.

The effect of shear flow is inadequate when the electric force and fluid flow have the same elevation (H = 0 cm); thus, no swirling occurs. Furthermore, different elevations ($H \neq$ 0 cm) influence the swirling flow direction differently.

Increasing the number of electrodes increases the electric field intensity and electrical voltage gradient. Consequently, the swirling flow becomes larger and stronger.

Acknowledgement

The researchers would like to thank the National Research University Project of the Office of Higher Education Commission of Thailand, the National Research Council of Thailand, and the Faculty of Engineering in Thammasat University for their financial support.

Nomenclature

b : Ion mobility (m^2/vs)
D : Electric flux density (C/m^2)
E : Electric field (V/m)
F_E : Electric force (C/m^2s)
H : Distance between electrode and ground in vertical direction (m)
J : Current density (A/m^2)
L : Distance between electrode and ground in horizontal direction (m)
n : Unit normal vector and coordinate in x and y axis
P : Pressure (N/m^2)
q : Space charge density (C/m^3)
T : Uniform temperature (K)
u : Inlet velocity (m/s)
V : Electrical voltage (V)

Greek letters

ε : Fluid permittivity (F/m)
η : Kinematic viscosity (m^2/s)
μ : Viscosity (kg/ms)
ρ : Density (kg/m^3)
ω : Vorticity (s^{-1})

Subscripts

in : Inlet
max : Maximum
0 : Atmospheric and wire
x, y : Axis

Superscript

T : Transpose of matrix

References

[1] P. Ratanadecho, K. Aoki and M. Akahori, Influence of irradiation time, particle sizes, and initial moisture content during microwave drying of multi-layered capillary porous materials, *J. Heat Transfer*, 124 (2002) 151-161.
[2] W. Cha-um, P. Rattanadecho and W. Pakdee, Experimental analysis of microwave heating of dielectric materials using a rectangular wave guide (MODE: TE10) (Case study: water layer and saturated porous medium), *Exp. Therm. Fluid Sci.*, 33 (2009) 472-481.
[3] N. Sakai and T. Hanzawa, Application and advances in infrared heating in Japan, *Trends Food Sci.Technol.*, 5 (11) (1994) 357-362.
[4] D. Nowak and P. P. Lewicki, Infrared drying of apple slices, *Innov. Food Sci. Emerg. Technol.*, 5 (2004) 353-360.
[5] S. D. Oh and H. Y. Kwak, Electrohydrodynamic (EHD) Enhancement of Boiling Heat Transfer of R 113 + WT4%

Ethanol, *J. Mech. Sci. and Tech.*, 20 (5) (2006) 681-691.
[6] N. Kasayapanand and T. Kiatsiriroat, Numerical modeling of the electrohydrodynamic effect to natural convection in vertical channels, *Int. Commun. Heat Mass Transfer*, 34 (2010) 162-175.
[7] B. S. Lee and J. S. Lee, A numerical study on electrohydrodynamic induction pumps using CFD modeling, *J. Mech. Sci. and Tech.*, 24 (11) (2010) 2207-2214.
[8] S. Saneewong Na Ayuttaya, C. Chaktranond, P. Rattanadecho and T. Kreewatcharin, Effect of ground arrangements on swirling flow in a channel subjected to electrohydrodynamic effects, *ASME J. Fluids Eng.*, 134, (2012) 051211-1-051211-10.
[9] N. Kasayapanand, Numerical study electrode bank enhanced heat transfer, *Appl. Therm. Eng.*, 26 (2006) 1471-1480.
[10] M. Huang and F. C. Lai, Numerical study of EHD-enhanced water evaporation, *J. Electrostatics*, 68 (2010) 364-370.
[11] C. Chaktranond and P. Ratanadecho, Analysis of heat and mass transfer enhancement in porous material subjected to electric fields (effects of particle sizes and layered arrangement), *Exp. Therm. Fluid. Sci.*, 34 (2010) 1049-1056.
[12] J. G. David, *Introduction to electrohydrodynamics*, Prentice Hall International, Inc. (1999).

S. Saneewong Na Ayuttaya is currently pursuing her Ph.D. in the Department of Mechanical Engineering of Thammasat University, Rangsit Campus, Thailand. She is presently involved in a numerical investigation on the enhancement of convective heat transfer by using electrohydrodynamic technique.

C. Chaktranond received his Ph.D. in 2006 from the Department of Mechanical Engineering of University of Tokyo, Japan. He is currently an associate professor at the Department of Mechanical Engineering of Thammasat University, Rangsit Campus, Thailand. His research interests are energy conservation in buildings and industrial plants and electrohydrodynamic drying.

P. Rattanadecho earned his Ph.D. in Mechanical Engineering in 2001 from Nagaoka University of Technology, Japan. He is currently a professor at the Department of Mechanical Engineering of Thammasat University, Thailand. His research interests include multi-phase flow in porous media under electromagnetic energy and transport phenomena in highly complex systems by using statistical modeling.